

# MEMS Based High Dose Radiation Resistant SOI Pressure Sensor for Aerospace Applications

Kyung Il Lee<sup>\*\*</sup>, M. M. Nayak<sup>3</sup>, Hidekuni Takao<sup>1,\*</sup>,  
Kazuaki Sawada<sup>2</sup>, Makoto Ishida<sup>2</sup> and K. Rajanna<sup>4</sup>

<sup>1</sup>Venture Business Laboratory, Toyohashi University of Technology,  
Hibarigaoka, Tempaku-Cho, Toyohashi 441-8580, Japan

<sup>2</sup>Department of Electrical and Electronic Engineering, Toyohashi University of Technology,  
Hibarigaoka, Tempaku-Cho, Toyohashi 441-8580, Japan

<sup>3</sup>LPSC, Indian Space Research Organization, 80 Feet Road, HAL 2<sup>nd</sup> Stage,  
Bangalore 5600 08, India

<sup>4</sup>Department of Instrumentation, Indian Institute of Science, Bangalore 560 012, India

(Received August 21, 2004; accepted December 3, 2004)

**Key words:** pressure sensors, SOI, radiation environment, microheaters

Transducers used in nuclear propulsion systems and space applications must withstand high-dose radiation environments along with high temperature operation. However, performance characteristics of various conventional silicon sensors are degraded at high temperature environments, and also show substantial radiation damage due to ionization in silicon. In this paper, a MEMS based high-dose radiation resistant SOI pressure sensor with integrated microheaters to maintain constant temperature for artificial satellites is developed, and its suitability for operation under high-dose radiation environment is reported. The developed sensor has inbuilt microheater arrangement for constant temperature operation. SOI pressure sensors were subjected to a radiation dosage level up to 100 krad, and performance characteristics such as linearity, offset and sensitivity were evaluated.

## 1. Introduction

Pressure sensors are in great demand for a variety of applications, such as industrial process control, gas turbine control systems, oil and gas exploration, aircraft flight test programs, nuclear propulsion systems and space applications. MEMS based devices with SOI structure are becoming attractive and have been reported.<sup>(1-3)</sup> Applying SOI technology to a working sensor is one of the means of raising the level of protection from the environment of the sensors under high temperatures.<sup>(4,5)</sup> In various application fields such as nuclear propulsion systems and aerospace applications, it is also necessary that pressure

---

\*Corresponding author, e-mail address: takao@eee.tut.ac.jp

\*\*Kyung Il Lee has transferred to the Research Institute of Industrial Science & Technology (RIST), #32 Hyoja-Dong, Nam-Ku, Pohang, 790-330 Kyungbuk, P.O.Box 135 Pohang, 790-600, Korea from February 1st, 2005.

sensors should be able to withstand a high-dose radiation environment. In this study, a MEMS-based SOI pressure sensor for operation under high-dose radiation environments is investigated, and the design and fabrication of SOI pressure sensors is carried out in view of their application to earth orbiting satellites, where sudden exposure to radiation from solar flares as well as normal gamma radiation is expected. Performance studies of the packaged SOI pressure sensors were carried out to determine output characteristics such as non linearity, hysteresis, and zero-offset drift. In order to evaluate its resistance to radiation, it was subjected to gamma radiation doses as high as 100 krad. The performance of sensors was also evaluated using an integrated microheater in order to reduce thermal drift.

## 2. Design and Fabrication

The cross section from A to B of the SOI pressure sensor is shown in Fig. 1(a), and the top view is shown in Fig. 1(b). It consists of the micromachined SOI silicon part and a glass part. The SOI piezoresistors to detect pressure are formed at the edges and center points of the diaphragm. The SOI piezoresistors are enclosed within the integrated microheaters, and SOI piezoresistors and the microheaters are formed using SOI active layers. Figures 2(a) and 2(b) show field-effect-modified (FEM) analysis of stress distribution on the

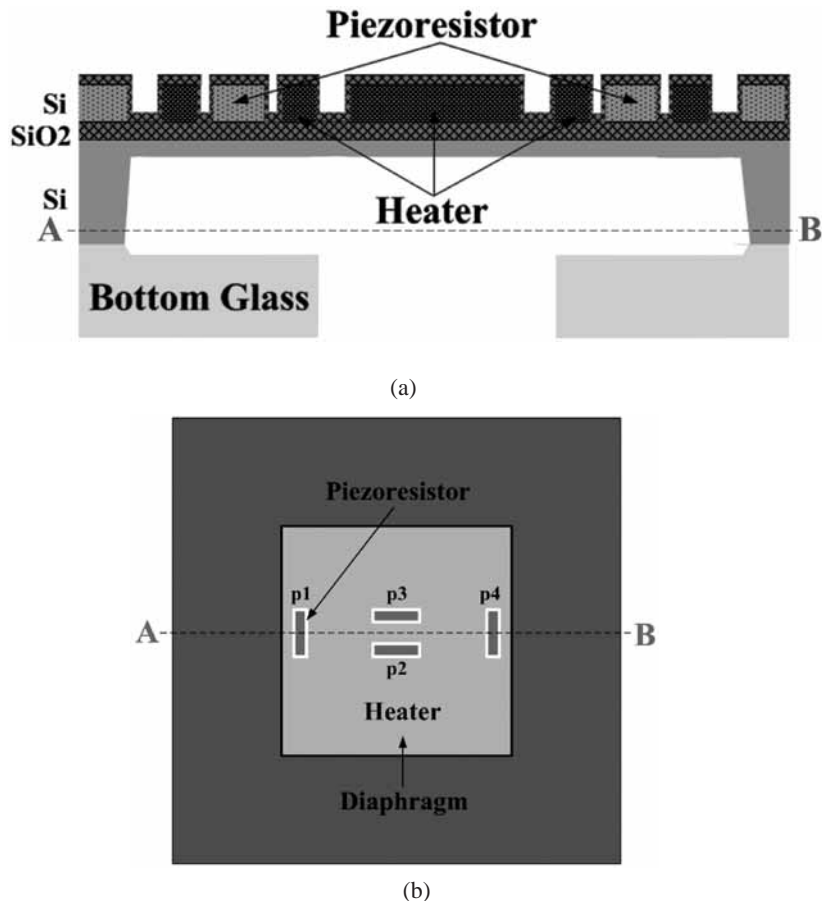
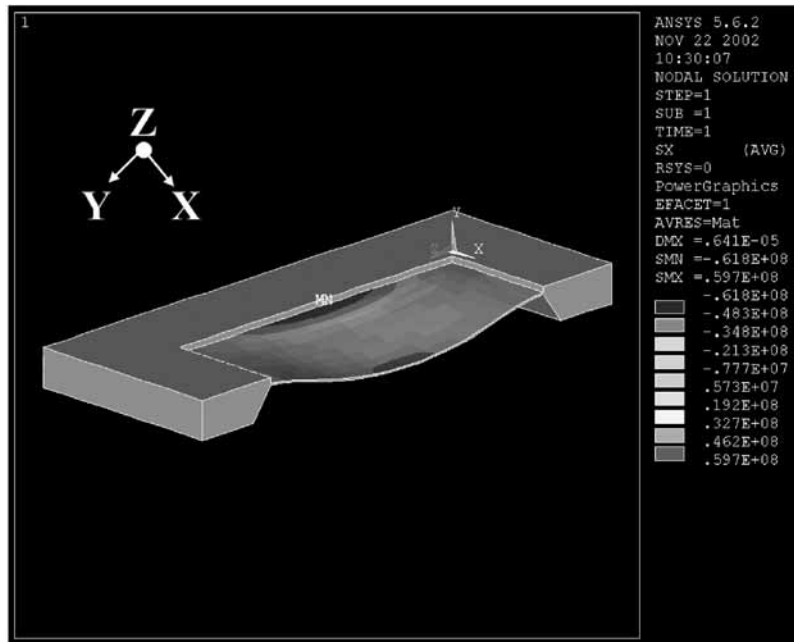
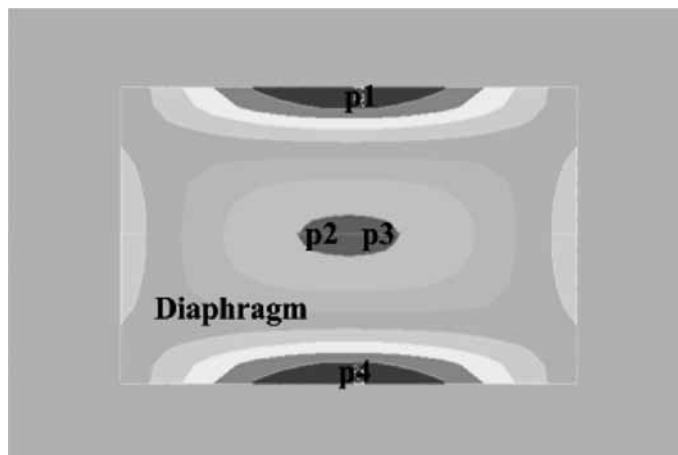


Fig. 1. Schematic of SOI pressure sensor. (a) Cross-sectional view. (b) Top view.

diaphragm. The position of the piezoresistors is optimized based on this result. As shown in Fig. 2, when the diaphragm is deflected downwards, the resistance of piezoresistor p2 and p3 on the center of diaphragm decreased and the resistance of piezoresistor p1 and p4 on the sides of the diaphragm increased. The piezoresistors of the pressure sensors are connected in the Wheatstone bridge configuration. The circuit configuration of pressure sensors with integrated microheaters is shown in Fig. 3.  $V_{WB}$  is the power supply of the Wheatstone bridge and  $V_H$  is the power supply to the integrated microheater. Because of



(a)



(b)

Fig. 2. FEM analysis of stress distribution on the diaphragm. (a) Cross-sectional diaphragm deflection. (b) Top view - p1, p2, p3 and p4 are the locations of the piezoresistors on the diaphragm.

the change in resistance of the piezoresistor values, the output voltages of the Wheatstone bridges increases or decreases from the initial balanced condition depending on diaphragm deflection direction. The maximum temperature of the pressure sensors is controlled for reduction of thermal drift at 200°C with constant temperature control systems using integrated microheaters. It is thought that the maximum temperature is sufficient to control the thermal drift of devices for satellite applications because the temperature of actual devices in a space satellite is never above 70°C. As a result, the operating temperature of SOI pressure sensors can be controlled at the desired operating temperature (the maximum temperature of sensor operation is 200°C in this study).

An SDB-SOI wafer consisting of 2.2  $\mu\text{m}$  active silicon, 1.1  $\mu\text{m}$   $\text{SiO}_2$  and 300  $\mu\text{m}$  substrate silicon is used as a starting material. In order to compare the output response of the pressure sensors by subjecting them to different doses of radiation, four different sizes of diaphragms with 15  $\mu\text{m}$  thickness are fabricated. The fabrication process steps of the SOI pressure sensors are shown in Fig. 4 and the details are as follows:

- (1) An SDB-SOI wafer of 2.2  $\mu\text{m}$  active-silicon, 1.1  $\mu\text{m}$   $\text{SiO}_2$  and 300  $\mu\text{m}$  substrate is used as the starting material.
- (2) The active silicon is entirely implanted with boron ( $1 \times 10^{18} \text{ cm}^{-3}$  concentration) to lower the sheet resistance value.
- (3) The masking layer is patterned and active-silicon is etched by reactive ion etching (RIE) to form island microheaters and piezoresistors for the pressure sensor.
- (4) Only the microheater region is implanted with boron ions to lower the sheet resistance value. The impurity (boron) concentration of the microheaters is  $1 \times 10^{20} \text{ cm}^{-3}$ .
- (5) A 15  $\mu\text{m}$  groove is formed by RIE to control the thickness of the diaphragm structure during the etching process using tetramethyl ammonium hydroxide (TMAH) solution. The aluminum layer is deposited by sputtering and patterned by wet etching.

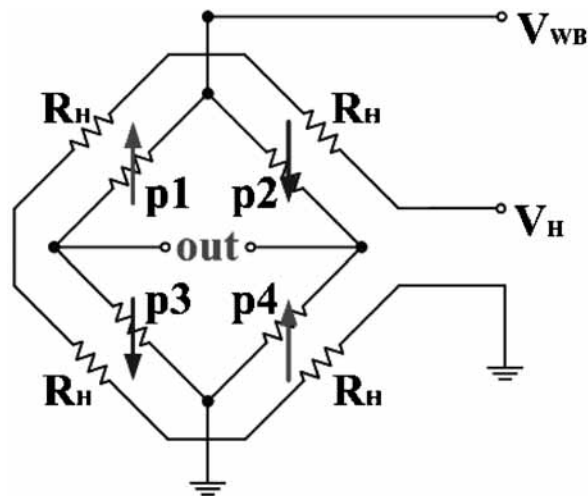


Fig. 3. Schematic of circuit configuration of pressure sensor with integrated microheater.

- (6) The aluminum layer is coated with fluorocarbon film.<sup>(4,6)</sup> This material is used as a passivation layer of the aluminum layer during the bulk silicon etching process using 25 wt.% TMAH solution.
- (7) The masking layer of the wafer backside is patterned, and bulk silicon is etched in TMAH solution at 90°C until the groove penetrates through the substrate.<sup>(7,8)</sup> Bulk silicon etching is carried out to achieve a 15- $\mu\text{m}$ -thick-diaphragm. After the etching, the backside masking layer was removed by HF solution.
- (8) The passivation layers are removed by O<sub>2</sub> plasma.
- (9) The bottom glass is patterned to achieve 1000- $\mu\text{m}$ -diameter holes with sandblasting.
- (10) After sandblasting, cleaning of the glass is carried out and the fabricated wafer and patterned glass are bonded with anodic bonding.

The individual sensors were diced and packaged for device testing and analysis. Figure 5 shows a photograph of the four such fabricated pressure sensor chips. The die size of the pressure sensors is 3 mm  $\times$  3 mm. The diaphragm sizes of Figs. 5(a), 5(b), 5(c) and 5(d) are 500  $\mu\text{m}$   $\times$  1500  $\mu\text{m}$   $\times$  15  $\mu\text{m}$ , 1000  $\mu\text{m}$   $\times$  1500  $\mu\text{m}$   $\times$  15  $\mu\text{m}$ , 500  $\mu\text{m}$   $\times$  500  $\mu\text{m}$   $\times$  15  $\mu\text{m}$  and 1000  $\mu\text{m}$   $\times$  1000  $\mu\text{m}$   $\times$  15  $\mu\text{m}$ , respectively. To make the pressure sensors either differential or gauge type, the glass to be bonded is fabricated using suitably designed masking layers to achieve 1000- $\mu\text{m}$ -diameter-holes with sandblasting. The photographs of packaged sensors are shown in Fig. 6.

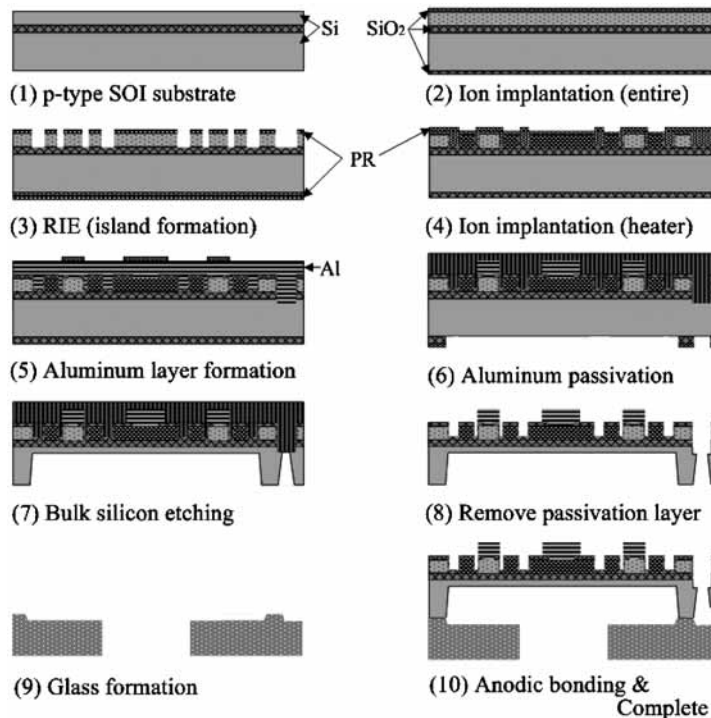


Fig. 4. Outline of fabrication process steps of the SOI pressure sensors.

### 3. Measured Characteristics

One of the packaged absolute-type pressure sensors having the dimensions  $500\ \mu\text{m} \times 500\ \mu\text{m} \times 15\ \mu\text{m}$  was initially calibrated using a pneumatic pressure controller (Model GPC-I of DH-Budenberg UK, accuracy 0.025%) to determine the nominal output, combined nonlinearity and hysteresis and only hysteresis. The sensor was subjected to radiation doses up to 100 krad in steps of 5 krad at a dose rate of 15 rad/s as per the MIL standard 750, condition 1039. A low-dose irradiator (Model 2000 of M/S BRIT, Mumbai, India, which is a compact, portable, self shielded type Cobalt-60 gamma source) was used for irradiating the sensor. In order to confirm the effectiveness of constant temperature control using the microheaters arrangement, a DC power supply for microheaters was used and the power level was maintained at 34 mW, 128 mW and 208 mW by adjusting the DC power supply voltages. Comparative output characteristic data for the pressure sensor with and without the microheaters arrangement is shown in Table 1. In these cases, it may be noted that the outer ambient temperature of the pressure sensor was at room temperature ( $\sim 20^\circ\text{C}$ ). Table 2 shows the data on the performance of the pressure sensor with the microheater power supply value at 208 mW and ambient temperature at two different values at  $50^\circ\text{C}$  and  $70^\circ\text{C}$ . It is evident from the data in Table 1 and Table 2 that the

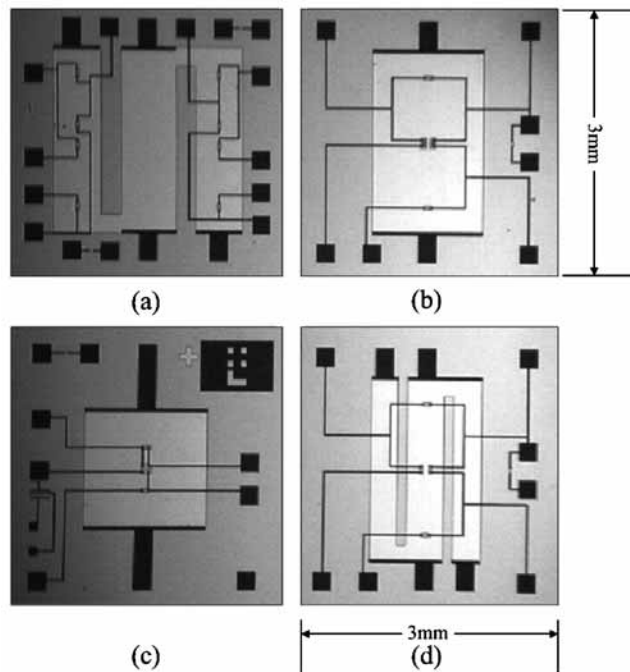


Fig. 5. Photographs of the fabricated SOI pressure sensor chip. (a) Differential type. (b), (c) and (d) Absolute type.



Fig. 6. Photographs of the packaged pressure sensors.

performance of the pressure sensor when the device is maintained with the integrated microheaters under ambient temperature  $\sim 20^{\circ}\text{C}$  is very much comparable to the performance (Full Scale Output (F.S.O.) and zero offset) with constant temperature control using the microheaters at  $50^{\circ}\text{C}$  and  $70^{\circ}\text{C}$  ambient temperature. The variations in full-scale output and zero offset with different ambient environmental temperatures when constant temperature control is performed with integrated microheaters are shown in Figs. 7 and 8, respectively. As can be seen Figs. 7 and 8, the variations are negligible. The overall difference in full-scale output as well as zero offset are 0.08% F.S.O. and 0.07% F.S.O., respectively. This clearly indicates the fact that the fabricated SOI pressure sensor is unaffected by the environmental temperature changes. Figure 9 shows the variation in radiation dosage versus zero offset up to 100 krad. As can be seen in Fig. 9, the SOI-based pressure sensor exhibits almost linear zero-offset variation. The calculated combined value of nonlinearity and hysteresis was below 0.5% of F.S.O. The post-irradiation calibration of the sensor indicated no noticeable change in nonlinearity, hysteresis or net output, and the sensitivity also remained unaltered. The performance was also measured after subjecting the sensor to  $70^{\circ}\text{C}$  for 3 h, because the temperature of actual devices in a space satellite is never above  $70^{\circ}\text{C}$ . Figure 10 shows the variation in sensor output with pressure for three different cases: before irradiation, after subject on irradiation dosage and after subject the sensor to  $70^{\circ}\text{C}$  for 3 h. As can be seen, the variation in sensor output after subjecting the sensor to  $70^{\circ}\text{C}$  for 3 h shows a positive shift of zero offset (0.001 V), which is negligible. However, the sensitivity remains the same before irradiation. The difference

in zero offset before and after the radiation test is about 0.016 V for up to 100 krad of radiation dose. The mechanical properties, such as Young's modulus and tensile strength, of the material used for the sensor are not affected by irradiation. Hence, sensitivity, linearity and full-scale-output remained unaltered. However, the observed zero-offset shift of the sensor is believed to be due to the fact that radiation causes a change in the mobility of carriers and hence alters the piezoresistance behavior.<sup>(9)</sup> It is thought that this shift might possibly be minimized by adopting appropriate shielding techniques.

#### 4. Conclusions

We have developed MEMS-based SOI pressure sensors and carried out experimental study on the suitability of these sensors for radiation environment applications. It has been observed that there was no significant change in linearity, hysteresis or sensitivity even

Table 1

Data on the performance of the pressure sensor with (constant temperature control is performed) and without (constant temperature control is not performed) the integrated microheater arrangement.

Parameters measured	Without microheaters	Constant temperature control is performed for sensors with microheaters		
		34 mW	128 mW	208 MW
Full-Scale Output (F.S.O.)	14.64 mV	14.61 mV	14.61 mV	14.55 mV
Zero Offset	699.10 mV	699.18 mV	699.21 mV	699.30 mV

Table 2

Data on the performance of the pressure sensor with constant temperature control when ambient temperature is varied from RT to 70°C.

Parameters measured	Ambient environmental temperatures		
	R.T.	50°C	70°C
Full-Scale Output (F.S.O.)	14.55 mV	14.60 mV	14.61 mV
Zero Offset	699.3 mV	699.24 mV	699.3 mV

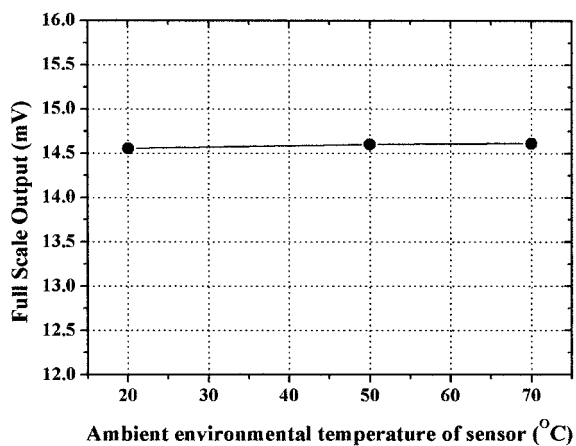


Fig. 7. Variation in Full-Scale output with different atmospheric temperatures when constant temperature control is performed with integrated microheaters.

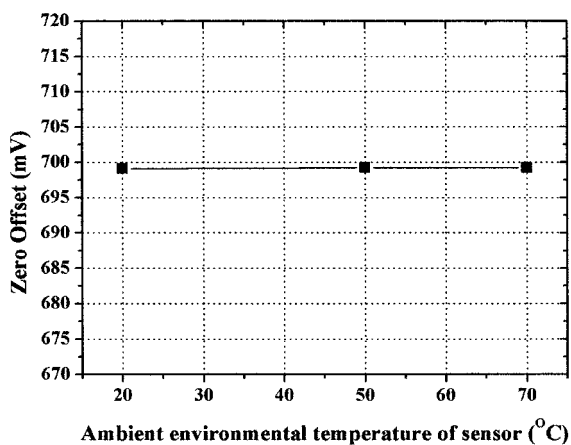


Fig. 8. Variation in zero offset with different atmospheric temperatures when constant temperature control is performed with integrated microheaters.

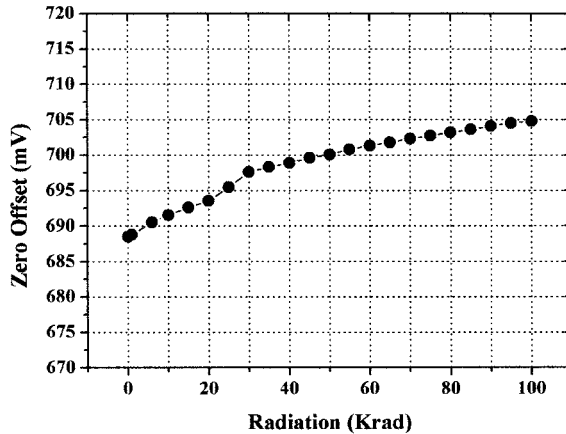


Fig. 9. Relationship between variation in radiation dosage and zero offset voltage.

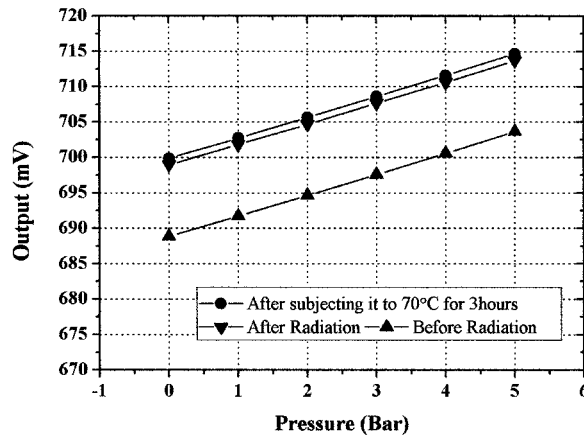


Fig. 10. Relationship of output voltage variation and pressure for different cases, namely, before radiation, after radiation and after subjecting the sensors to 70°C for 3 h.

after subjecting the sensor to gamma radiation doses as high as 100 krad. However, the observed zero-offset shift of the sensor is about 0.016 V at the maximum dosage level (100 krad). It is thought that the zero-offset shift might possibly be minimized by adopting appropriate shielding techniques, since the shift is linear. The performance of sensors was also evaluated using an integrated microheater in order to reduce thermal drift. It is also important to note that the integration of the microheaters eliminates the need for additional thermal compensation circuits. The above observations indicate that the developed MEMS-based SOI-structured pressure sensor can be used for applications under radiation environment up to a dosage level of almost 100 krad.

### Acknowledgement

This work was supported by the Venture Business Laboratory at Toyohashi University of Technology and The 21<sup>st</sup> Century COE Program “Intelligent Human Sensing,” from the Ministry of Education, Culture, Sports, Science and Technology, Japan.

### References

- 1 Y. T. Lee, H. D. Seo, M. Ishida, S. Kawashita and T. Nakamura: Sensors and Actuators A **43** (1994) 59.
- 2 H. Takao, Y. Matsumoto, H. D. Seo, M. Ishida and T. Nakamura: Sensors and Actuators A **55** (1996) 91.
- 3 M. Ishida: J. Indian Inst. Sci. **81** (2001) 619.
- 4 K. I. Lee, H. Takao, K. Sawada and M. Ishida: Sensors and Actuators A **104** (2003) 53.
- 5 L. R. Hite, H. Lu, T. W. Houston, D. S. Hurta and W. E. Bailey: IEEE Trans. Nucl. Sci. **39** (1992) 2121.
- 6 H. Takao, Y. Matsumoto and M. Ishida: IEEE Trans. Electron Devices **46** (1999) 109.
- 7 O. Tabata, R. Asahi, H. Funabashi, K. Shimaoka, S. Su: Sensors and Actuators A **34** (1992) 51.
- 8 H. Takao, Y. Matsumoto, M. Ishida: IEE Japan, PS 96-**14**, (1996) 71.
- 9 T. P. Ma and Paul V. Dressendorfer, Ionizing Radiation Effects in MOS Devices and Circuits (John Wiley & Sons Inc., 1989)